ASTREV 845
19 October 2004; Disk Used

ARTICLE IN PRESS

No. of Pages 13, DTD = 5.0.1

Available online at www.sciencedirect.com

SCIENCE DIRECT®

ELSEVIER

New Astronomy Reviews xxx (2004) xxx–xxx

New Astronomy Reviews

www.elsevier.com/locate/newastrev

Late stages of stellar evolution

Kevin Marvel

American Astronomical Society, 2000 Florida Avenue, NW, Suite 400, Washington, DC 20009, USA

Abstract

The square kilometer array (SKA) will have the sensitivity, spatial resolution, and frequency resolution to provide new scientific knowledge of evolved stars. Four basic areas of scientific exploration are enhanced by the construction of the SKA: (1) detection and imaging of photospheric radio continuum emission and position correlation with maser distributions, (2) imaging of thermal dust emission around evolved stars and the detailed structures of their circumstellar winds (again, including comparison with maser distributions), (3) study of cm-wavelength molecular line transitions and the circumstellar chemistry around both O-rich and C-rich evolved stars and (4) the possible observation of polarized emission due to the influence of the magnetic fields of AGB stars. Since this short chapter is not meant to be a review article, a comprehensive reference list has not been generated. I have selected just one or perhaps two references for citations where appropriate.

1. Introduction

Although much can be learned by studying stellar nurseries and the fascinating process of stellar birth, we have much yet to learn in the field of stellar geriatrics. Stars that do not proceed to explosive ends, the low- and intermediate-mass stars, undergo a period of mass loss, often extreme, in which 50% or more of the star's initial mass is transferred back to the ISM. The rates of this mass loss vary widely from $10^{-6} M_{\odot}$ per year to as much as $10^{-4} M_{\odot}$ per year.

Such prodigious mass loss and the large number of low- and intermediate-mass stars results in the fact that most of the interstellar medium – perhaps as much as 80–90% – has been cycled through a star and ejected via this process. Flash-in-the-pan supernovae do have a significant impact, especially enriching the heavier metals in the ISM, but the bulk of the material is provided by the aging process of common stars similar to the Sun. Understanding how the mass loss process proceeds and its implications on the chemical modification of the ISM in our own galaxy has obvious implica-

E-mail address: marvel@aas.org.

1387-6473/$ - see front matter
doi:10.1016/j.newar.2004.09.042

ASTREV 845
19 October 2004; Disk Used
ARTICLE IN PRESS
No. of Pages 13, DTD=5.0.1

tions for the study of more distant galaxies as well as being of interest itself.

The mass loss process proceeds from the formation of dust in the upper atmospheres of evolved stars, a few stellar radii from the optical photosphere. This process has long been thought to be driven by the pulsations inherent in these kinds of stars, but it now appears likely that it is driven by dramatic temperature fluctuations caused by the formation of TiO in the stellar atmosphere, which changes the physical conditions in the dust formation region (Reid and Goldston, 2002).

Although the details of dust formation remain an unknown factor, we know roughly that when the temperature and density conditions are appropriate, nucleation can occur, leading to the formation of dust. This dust, exposed to the radiation field of the evolved star, absorbs outward momentum and begins to accelerate. Gas not incorporated into dust grains is carried along with the dust through momentum coupling. As conditions allow, molecules can form from the gas that is carried along with the outward-moving dust. Using existing centimeter and millimeter wave interferometers, studies of the molecules formed in these winds have been completed showing more or less spherically symmetric mass loss (Rieu and Bieging, 1990) with some interesting results such as rotation (Bieging and Rieu, 1996) and perfect spherical symmetry of an apparently single ejection event (Olofsson et al., 1998).

Certain molecules are capable of maser emission (e.g. SiO, H_2O and OH). When such masers are found in the winds of evolved O-rich stars, they are powerful probes of the mass loss kinematics. Some C-rich stars do exhibit HCN masers at high frequencies, but the O-dominated species are absent. However, they can provide only rough information about the physical conditions of the wind itself, provided by the physical conditions required for maser emission. Using VLBI techniques, which provide resolutions as fine as 100 μas, the motions of masing gas can be tracked with high accuracy and the kinematics of the wind modelled. In practice, this has proven to be a challenging undertaking. The non-linear emission process and apparently complex distributions of the masers make modelling difficult. Only rough models have yet been made placing the masers in ellipsoidal distributions undergoing a variety of kinematic motions. The maser observations do indicate more-or-less spherically or elliptically symmetric mass loss with acceleration occurring to the outermost regions of the wind where acceleration ceases due to decoupling of the gas from the dust. A mild controversy about the relative angular scales of the OH and H_2O maser distributions (e.g. the OH masers, although predicted to be at large radii, appear at about the same angular scale as the H_2O masers) is likely due to beaming effects. Water masers are preferentially tangentially beamed as they reside in an accelerating portion of the wind while the OH masers are radially beamed as they reside in a constant velocity region of the wind (Reid, 2002). As difficult as the physics and geometries are, our current understanding is limited due to lack of adequate modelling in my opinion. Other results indicate non-negligible rotation (Boboltz and Marvel, 2000) of the envelopes and the influence of magnetic fields on the shape of the shell (Murakawa et al., 2003).

We have yet to understand the dust formation process in these objects. Although infrared interferometric observations (Monnier et al., 2004) hint at a very clumpy and dynamic process, we have few tools available to probe this process in detail. We have only a very rough picture of the structure of the extended photosphere and wind of evolved stars. The role of magnetic fields in AGB stars has not been explored in any detail, though they must impact the dust formation process, the wind itself and obviously provide information on the star itself.

Although detailed studies have been made using millimeter interferometers of the chemical structure of the nearest and largest evolved stars, much of the chemical structure in these objects remains a mystery. ALMA will help here but will miss the low-frequency line transitions. A detailed understanding of the structure of these objects awaits the square kilometer array (SKA).

The SKA, with its high resolution, sensitivity to a range of emission mechanisms and low-frequency observing capability will allow studies of evolved stars that have not been possible before and provide complementary observations to those provided by ALMA and other instruments. I discuss the anticipated observations SKA can provide in the sections below.

2. Imaging the surfaces of AGB stars

2.1. Fluctuations first

It has been shown (Petit and Nicholson, 1933) that certain AGB stars, the Mira variables, undergo temperature changes of 30% and luminosity changes of a factor of two during their visual fluctuation period ($L = \sigma T_e^4 \pi R^2$). As shown in Reid and Goldston (2002), these changes should result in stellar radius fluctuations of about 40%. Such dramatic fluctuations would lead to both dramatic shock waves that propagate from the star into its extended photosphere and also measurable changes in light curves at radio, infrared and optical wavelengths. The visual light curve fluctuates dramatically (extreme cases show fluctuations of 8 magnitudes) while the infrared light curves rarely fluctuate by more than a magnitude and the radio light curves fluctuate only by a few percent at most.

Observed light curves do not match those predicted by the radial fluctuations implied by the temperature and luminosity fluctuations (Reid and Goldston, 2002). Fig. 1 shows the model from (Reid and Goldston (2002)) that (to first order) reproduces the radio, infrared and visual light curves. The model predicts that TiO is formed in the upper atmosphere as the star approaches minimum light and this additional opacity source can greatly decrease the observed light at visual wavelengths while having less impact at infrared wavelengths and almost no impact at radio wavelengths. This new discovery shows that much remains to be learned about evolved stars. After all, Mira variables are one of the oldest astronomical phenomena studied and only now has an adequate first-order model been developed to explain their fluctuations.

The SKA will allow further testing of these models at far greater sensitivity. Observations of

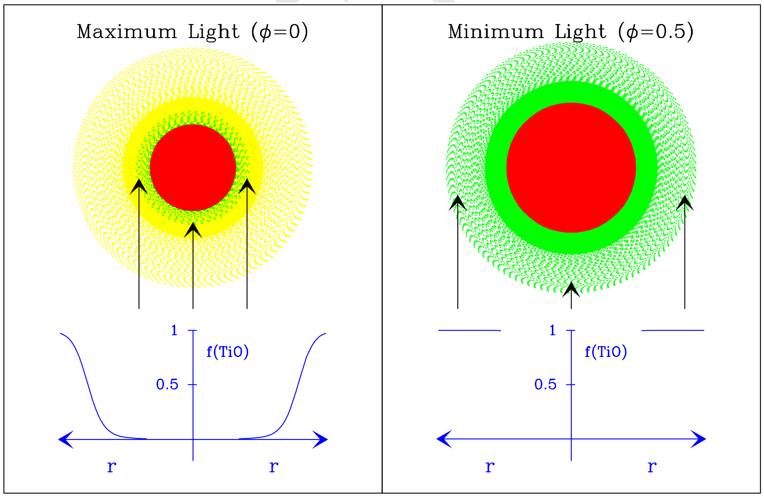

Fig. 1. A schematic depiction of the change in visual appearance of a Mira variable star at maximum (left-hand panel) and minimum (right-hand panel) light. The star, shown in red, is smaller and hotter at maximum light than at minimum light. At maximum light, the extended atmosphere of the star (shown as yellow) is partially transparent at visual wavelengths, and one sees almost down to the stellar surface (indicated with arrows). Near minimum light, the temperature of the star has declined and metallic oxides, such as TiO (shown as green), form throughout the extended atmosphere. The fraction of Ti in TiO, *f*(TiO), as a function of radius is plotted in blue. Near minimum light, TiO forms with sufficient density at a radius of $\approx 1.8 R_*$ to become opaque to visible light. At this radius, the temperature can be very low, and almost all radiation is in the infrared. Since little visible light emerges, the star can almost disappear to the human eye. Figure and caption text taken from Reid and Goldston (2002).

the flux from the photospheres of AGB stars are exceedingly difficult. Typical fluxes are on the order of 200 μJy and require special calibration techniques with current interferometers. The SKA, with a sensitivity of about 0.1 μJy at 20 GHz will provide the most accurate AGB star light curves across all wavelengths. Such measurements will allow improved modelling of the opacity source fluctuations in the star.

The discovery of particularly large extrasolar planets orbiting close to their host star opens up the possibility for the observation of eclipses using the SKA, as has been observed in the star HD 209458. However, the eclipse type that is potentially observable would be an active radio-emitting planet similar to Jupiter being eclipsed by its host star rather than the more typical eclipse. As pointed out in Taylor and Braun (1999), Jupiter-like planets will produce detectable radio emission out to distances of 10 pc. The passage of a planet of this type behind its host AGB star would be detectable, since the emission from the planet would be of order 10 μJy, compared to the photospheric flux of 200 μJy.

2.2. Imaging second

The diameter of the radio photosphere of a typical AGB star is of order 5 AU. At 1 kpc, such a source would have a maximum angular diameter of 6 mas. At 22 GHz and with 1000 km baselines, the SKA will have a resolution of roughly 3 mas. This resolution corresponds to linear resolution of 3 AU at 1 kpc. For AGB star diameters of 3–5 AU, they can be moderately resolved with SKA. Thus, for only the nearest AGB stars will any degree of imaging be possible. The number of AGB stars closer than 1 kpc is limited. Without a substantial increase in the highest frequency observed by the SKA or the maximum baselines, imaging of only the nearest AGB stars will be possible.

That said, some very interesting imaging projects can be undertaken for large AGB stars not further than 1 kpc from the Earth. For example, the well-known and nearby (150 pc) carbon star IRC + 10216 has a photospheric size of 35 mas and an extended envelope diameter of nearly 1′. With a resolution element of 3 mas, the surface of the star would be imaged well and the overall envelope, especially in spectral lines (see below) would be highly resolved. The imaging design goal of 0.1″ resolution at 1.4 GHz over a 1° field (and scaled with frequency) is sufficient to provide high spatial dynamic range imaging at high sensitivity for objects of this type. The science the SKA will allow is the direct imaging of the dust formation process and connection with stellar pulsation for the nearest and largest AGB stars.

3. Observations of masers and their host stars

Maser emission from gas in the outflowing winds of AGB stars is a common phenomenon in O-rich AGB stars. Masers are regions of gas in the stellar wind that have sufficient velocity coherence to amplify background photons via amplified emission of radiation. Such amplification is possible due to a population inversion of the molecular species in question and a fortuitous alignment of molecular rotational, vibrational or ro-vibrational energy levels. Several species are found. SiO masers are located close to the star (within a few stellar radii and below the dust formation zone). H_2O masers are located at intermediate distances from a few tens of stellar radii to a few hundred. The remote OH masers are located up to several thousand stellar radii from the host star.

In addition to knowing the location of the various maser species, we have a good understanding of the overall shell structure around these stars (Reid, 2002). Fig. 2 shows graphically our current understanding of the circumstellar region around an AGB star. The star itself is from between 1 and 5 AU in size. Above this surface is a chromospheric region followed by a molecular photosphere ending between 1 and 2 AU above the optical photosphere. The radio photosphere (about 0.5–1 AU in thickness) is located near the SiO maser formation region. Beyond this zone, wind acceleration begins as dust forms in a region from roughly 5 to 10 AU (depending on the properties of the star and pulsation phase). The H_2O and OH masers begin to appear at radii of 15 AU or more and the OH masers are found further out

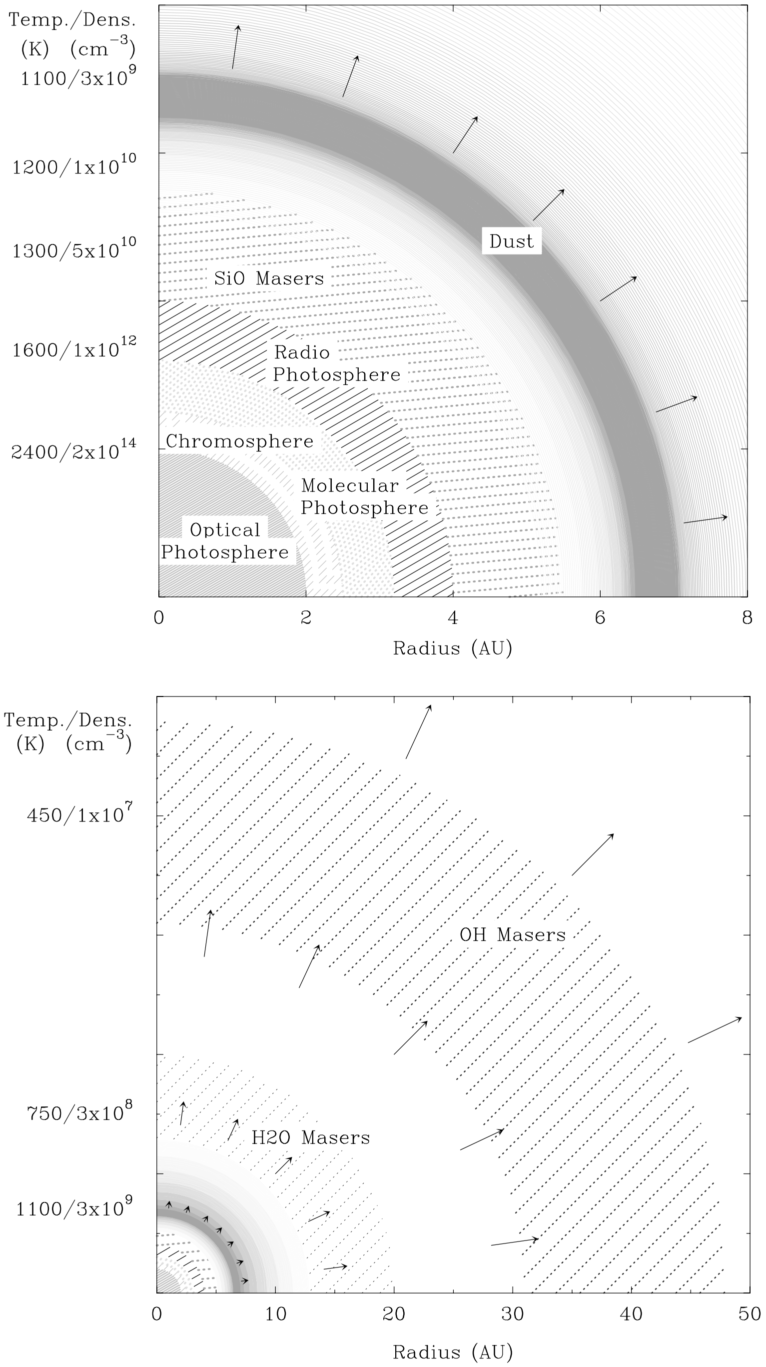

Fig. 2. A schematic showing our current understanding of the circumstellar region around an AGB star (Reid, 2002).

from the water maser shell. The exact sizes of the various regions, their exact locations and how they interact remain rough measurements.

Masers are imaged using VLBI techniques and typically have resolved sizes of a milliarcsecond or so, but observations with MERLIN show that a weak diffuse emission can also be present (Richards et al., 1999). Depending on the upper frequency cutoff for the SKA, the OH (1.6 GHz), methanol (6.7 GHz) and water masers (22 GHz) could be observable. However, it is not the detection of maser emission with the SKA that is of greatest interest (though the sensitivity of the instrument would allow detection of extragalactic masers to a much greater distance than currently available). It is the sensitivity to both the stellar photospheric emission and the dust continuum in the wind combined with the VLBI observations that will be of prime interest.

VLBI imaging techniques are sensitive only to very high brightness temperatures and the smallest angular sizes (1–5 mas) and therefore only the maser spots themselves and not the environment in which they are located can be imaged. With the angular resolution of the SKA at 1.4 GHz (0.1″), the thermal emission across a typical OH maser distribution 1–2″ in diameter could be mapped with sufficient resolution and sensitivity to allow alignment of the VLBI maser observations with the overall dust distribution and star itself. Combined with infrared interferometric observations, which are now beginning to show the details of the dust distribution at high angular resolutions (see Fig. 3) (Monnier et al., 2004) (≈10 mas, but over limited fields of view), the SKA will play a critical role in providing information on the largest scales.

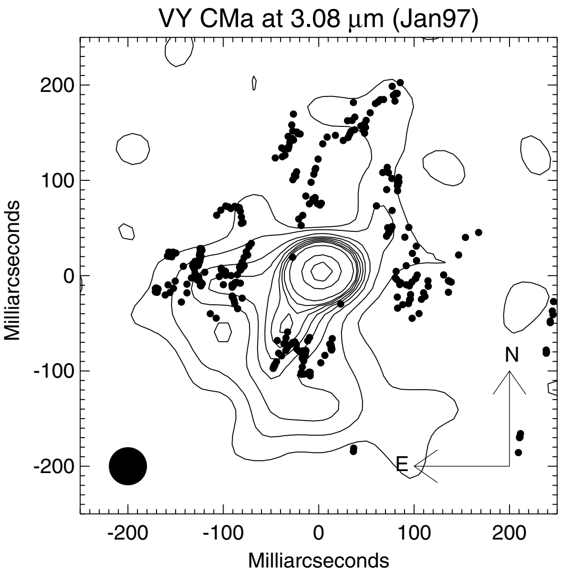

Fig. 3. This figure shows the locations of water masers detected with MERLIN (note beamsize of 40 mas in lower left-hand corner of figure) overlaid on infrared emission at 3.08 μm. The infrared emission was imaged using an interferometric masking technique on the Keck 10 m telescope. Although registration of the images is a challenge technically, the image shows the power of such combination observations. Multi-epoch observations of both the water masers and the infrared emission shows changes over time and there is some hope of making time-lapse movies of these sources in the future. Figure courtesy of J. Monnier. (Monnier et al., 1999; Richards et al., 1998).

Outstanding problems to be addressed include the details of dust formation, such as whether the process proceeds uniformly as a function of pulsation cycle or at particular times, the degree of clumpiness of the dust formation and the exact physical conditions that lead to dust formation. The transition of AGB stars from roughly spherically symmetric mass-losing objects to the asymmetric planetary nebulae has yet to be understood completely and the combination of the kinematic information provided by VLBI maser observations and the dust distribution will hopefully shed new light on this area.

4. Molecular gas

In the frequency range of the SKA are 634 molecular line transitions, many of which have not been well-studied, only detected, and some of which have still not been identified (Lovas, 2002). For convenience, these transitions are provided in Table 1 .

Many of these species are expected to be present in the winds of evolved stars. As pointed out by Zijlstra (2003), both the dust and gas created in the stellar winds of AGB stars survive in the ISM. The dust, as indicated by reddening and particles found in meteorites or as micrometeoroid particulates in our own upper atmosphere (Messenger et al., 2003), survives in interstellar space. The presence of the diffuse interstellar bands are the main piece of evidence for the existence of rather complex molecules in interstellar space. As yet, we do not know if the molecules were formed

Table 1
Molecular line transitions in the frequency range 700 MHz to 30 GHz detected at least once in the interstellar environment Lovas, 2002

Frequency (MHz)	Formula	Quantum numbers
701.679	CH	23/2 J = 3/2 F = 2–2
704.175	CH	23/2 J = 3/2 F = 2+−1−
722.303	CH	23/2 J = 3/2 F = 1+−2−
724.791	CH	23/2 J = 3/2 F = 1–1
834.285	CH_3OH	1(1,0)–1(1,1) A−+
1065.076	CH_3CHO	1(1,0)–1(1,1) A−+
1371.722	CH_2CHCN	2(1,1)–2(1,2) F = 1–1
1371.797	CH_2CHCN	2(1,1)–2(1,2) F = 3–3
1371.934	CH_2CHCN	2(1,1)–2(1,2) F = 2–2
1538.108	NH_2CHO	1(1,0)–1(1,1) F = 1–1
1538.676	NH_2CHO	1(1,0)–1(1,1) F = 1–2
1539.264	NH_2CHO	1(1,0)–1(1,1) F = 2–1
1539.527	NH_2CHO	1(1,0)–1(1,1) F = 1–0
1539.832	NH_2CHO	1(1,0)–1(1,1) F = 2–2
1540.998	NH_2CHO	1(1,0)–1(1,1) F = 0–1
1570.805	$NH_2{}^{13}CHO$	1(1,0)–1(1,1) F = 2–2
1584.274	^{18}OH	23/2 J = 3/2 F = 1–2
1610.247	CH_3OCHO	1(1,0)–1(1,1) A
1610.900	CH_3OCHO	1(1,0)–1(1,1) E
1612.2310	OH	23/2 J = 3/2 F = 1–2
1624.518	^{17}OH	23/2 J = 3/2 F,F1=7/2,4–7/2,4
1626.161	^{17}OH	23/2 J = 3/2 F,F1=9/2,4–9/2,4
1637.564	^{18}OH	23/2 J = 3/2 F = 1–1
1638.805	HCOOH	1(1,0)–1(1,1)
1639.503	^{18}OH	23/2 J = 3/2 F = 2–2
1665.4018	OH	23/2 J = 3/2 F = 1–1
1667.3590	OH	23/2 J = 3/2 F = 2–2
1692.795	^{18}OH	23/2 J = 3/2 F = 2–1
1720.5300	OH	23/2 J = 3/2 F = 2–1
2661.61	HC_5N	1–0 F = 1–1
2662.87	HC_5N	1–0 F = 2–1
2664.76	HC_5N	1–0 F = 0–1
3139.404	H_2CS	2(1,1)–2(1,2)
3195.162	CH_3CHO	2(1,1) – 2(1,2) A−+
3263.794	CH	21/2 J = 1/2 F = 0–1
3335.481	CH	21/2 J = 1/2 F = 1–1
3349.193	CH	21/2 J = 1/2 F = 1–0
4388.7786	$H_2C^{18}O$	1(1,0)–1(1,1) F = 1–0
4388.7960	$H_2C^{18}O$	1(1,0)–1(1,1) F = 0–1
4388.7963	$H_2C^{18}O$	1(1,0)–1(1,1) F = 2–2
4388.8011	$H_2C^{18}O$	1(1,0)–1(1,1) F = 2–1
4388.8035	$H_2C^{18}O$	1(1,0)–1(1,1) F = 1–2
4388.8084	$H_2C^{18}O$	1(1,0)–1(1,1) F = 1–1
4592.9563	$H_2{}^{13}CO$	1(1,0)–1(1,1)1/2,1/2–1/2,3/2
4592.9738	$H_2{}^{13}CO$	1(1,0)–1(1,1)1/2,1/2–3/2,3/2
4592.9759	$H_2{}^{13}CO$	1(1,0)–1(1,1)3/2,1/2–1/2,3/2
4592.9857	$H_2{}^{13}CO$	1(1,0)–1(1,1)3/2,1/2–5/2,3/2
4592.9934	$H_2{}^{13}CO$	1(1,0)–1(1,1)3/2,1/2–3/2,3/2
4593.0494	$H_2{}^{13}CO$	1(1,0)–1(1,1)1/2,1/2–1/2,1/2
4593.0690	$H_2{}^{13}CO$	1(1,0)–1(1,1)3/2,1/2–1/2,1/2

Table 1 (continued)

4593.0800	$H_2{}^{13}CO$	1(1,0)–1(1,1)1/2,1/2–3/2,1/2
4593.0812	$H_2{}^{13}CO$	1(1,0)–1(1,1)1/2,3/2–1/2,3/2
4593.0864	$H_2{}^{13}CO$	1(1,0)–1(1,1)3/2,3/2–1/2,3/2
4593.0865	$H_2{}^{13}CO$	1(1,0)–1(1,1)5/2,3/2–5/2,3/2
4593.0942	$H_2{}^{13}CO$	1(1,0)–1(1,1)5/2,3/2–3/2,3/2
4593.0961	$H_2{}^{13}CO$	1(1,0)–1(1,1)3/2,3/2–5/2,3/2
4593.0985	$H_2{}^{13}CO$	1(1,0)–1(1,1)1/2,3/2–3/2,3/2
4593.0994	$H_2{}^{13}CO$	1(1,0)–1(1,1)3/2,1/2–3/2,1/2
4593.1039	$H_2{}^{13}CO$	1(1,0)–1(1,1)3/2,3/2–3/2,3/2
4593.1741	$H_2{}^{13}CO$	1(1,0)–1(1,1)1/2,3/2–1/2,1/2
4593.1795	$H_2{}^{13}CO$	1(1,0)–1(1,1)3/2,3/2–1/2,1/2
4593.2003	$H_2{}^{13}CO$	1(1,0)–1(1,1)5/2,3/2–3/2,1/2
4593.2046	$H_2{}^{13}CO$	1(1,0)–1(1,1)1/2,3/2–3/2,1/2
4593.2099	$H_2{}^{13}CO$	1(1,0)–1(1,1)3/2,3/2–3/2,1/2
4617.121	NH_2CHO	2(1,1)–2(1,2) F = 2–2
4618.967	NH_2CHO	2(1,1)–2(1,2) F = 3–3
4619.993	NH_2CHO	2(1,1)–2(1,2) F = 1–1
4660.242	OH	21/2 J = 1/2 F = 0–1
4750.656	OH	21/2 J = 1/2 F = 1–1
4765.562	OH	21/2 J = 1/2 F = 1–0
4829.6412	H_2CO	1(1,0)–1(1,1) F = 1–0
4829.6587	H_2CO	1(1,0)–1(1,1) F = 0–1
4829.6594	H_2CO	1(1,0)–1(1,1) F = 2–2
4829.6639	H_2CO	1(1,0)–1(1,1) F = 2–1
4829.6664	H_2CO	1(1,0)–1(1,1) F = 1–2
4829.6710	H_2CO	1(1,0)–1(1,1) F = 1–1
4916.312	HCOOH	2(1,1)–2(1,2)
5005.3208	CH_3OH	3(1,2)–3(1,3) A−+
5289.015	CH_2NH	1(1,0)–1(1,1) F = 0–1
5289.678	CH_2NH	1(1,0)–1(1,1) F = 1–0
5289.813	CH_2NH	1(1,0)–1(1,1) F = 2–2
5290.614	CH_2NH	1(1,0)–1(1,1) F = 2–1
5290.879	CH_2NH	1(1,0)–1(1,1) F = 1–2
5291.680	CH_2NH	1(1,0)–1(1,1) F = 1–1
5324.058	HC_5N	2–1 F = 2–2
5324.270	HC_5N	2–1 F = 1–0
5325.330	HC_5N	2–1 F = 2–1
5325.421	HC_5N	2–1 F = 3–2
5327.451	HC_5N	2–1 F = 1–1
6016.746	OH	23/2 J = 5/2 F = 2–3
6030.747	OH	23/2 J = 5/2 F = 2–2
6035.092	OH	23/2 J = 5/2 F = 3–3
6049.084	OH	23/2 J = 5/2 F = 3–2
6278.628	H_2CS	3(1,2)–3(1,3)
6389.933	CH_3CHO	3(1,2)–3(1,3) A−+
6668.5192	CH_3OH	5(1,6)–6(0,6) A++
7761.747	OH	21/2 J = 3/2 F = 1–1
7820.125	OH	21/2 J = 3/2 F = 2–2
7895.989	HC_7N	7–6 F = 6–5
7896.010	HC_7N	7–6 F = 7–6
7896.023	HC_7N	7–6 F = 8–7
7987.782	HC_5N	3–2 F = 2–1
7987.994	HC_5N	3–2 F = 3–2
7988.044	HC_5N	3–2 F = 4–3

(continued on next page)

Table 1 (*continued*)

Frequency (MHz)	Formula	Quantum numbers
8135.870	OH	21/2 J = 5/2 F = 2–2
8189.587	OH	21/2 J = 5/2 F = 3–3
8775.088	CH_3NH_2	2(0,2)–1(0,1) F = 1–0 Aa
8777.442	CH_3NH_2	2(0,2)–1(0,1) F = 3–2 Aa
8778.200	CH_3NH_2	2(0,2)–1(0,1) F = 2–2 Aa
8778.260	CH_3NH_2	2(0,2)–1(0,1) F = 1–1 Aa
8779.496	CH_3NH_2	2(0,2)–1(0,1) F = 2–1 Aa
8815.814	$H^{13}CCCN$	1–0 F = 1–1
8817.096	$H^{13}CCCN$	1–0 F = 2–1
8819.019	$H^{13}CCCN$	1–0 F = 0–1
9024.009	HC_7N	8–7
9058.447	$HC^{13}CCN$	1–0 F = 1–1
9059.318	$HCC^{13}CN$	1–0 F = 1–1
9059.736	$HC^{13}CCN$	1–0 F = 2–1
9060.6080	$HCC^{13}CN$	1–0 F = 2–1
9097.0346	HCCCN	1–0 F = 1–1
9098.3321	HCCCN	1–0 F = 2–1
9100.2727	HCCCN	1–0 F = 0–1
9118.823	CH_3OCH_3	2(0,2)–1(1,1) AA
9119.671	CH_3OCH_3	2(0,2)–1(1,1) EE
9120.509	CH_3OCH_3	2(0,2)–1(1,1) AE
9120.527	CH_3OCH_3	2(0,2)–1(1,1) EA
9235.119	NH_2CHO	3(1,2)–3(1,3) F = 3–3
9237.034	NH_2CHO	3(1,2)–3(1,3) F = 4–4
9237.704	NH_2CHO	3(1,2)–3(1,3) F = 2–2
9486.71	Unidentified	
9493.061	C_4H	3/2–1/2 F = 1–0
9496.4	Unidentified	
9497.616	C_4H	3/2–1/2 F = 2–1
9508.005	C_4H	3/2–1/2 F = 1–1
9547.953	C_4H	1/2–1/2 F = 1–0
9551.717	C_4H	1/2–1/2 F = 0–1
9562.904	C_4H	1/2–1/2 F = 1–1
9703.508	C_6H	23/2 J = 3.5–2.5 F = 4–3 e
9703.600	C_6H	23/2 J = 3.5–2.5 F = 3–2 e
9703.835	C_6H	23/2 J = 3.5–2.5 F = 4–3 f
9703.936	C_6H	23/2 J = 3.5–2.5 F = 3–2 f
9877.606	HC_9N	17–16
9885.89	CCCN	1–0 J = 3/2–1/2 F = 5/2–3/2
9936.202	CH_3OH	9(−1,9)–8(−2,7) E
9978.686	CH_3OH	4(3,2)–5(2,3) E
10058.257	CH_3OH	4(3,1)–5(2,4) E
10152.008	HC_7N	9–8
10278.246	HDO	2(2,0)–2(2,1)
10458.639	HC_9N	18–17
10463.962	H_2CS	4(1,3)–4(1,4)
10648.419	CH_3CHO	4(1,3)–4(1,4) A−+
10650.563	HC_5N	4–3 F = 3–2
10650.654	HC_5N	4–3 F = 4–3
10650.686	HC_5N	4–3 F = 5–4
11119.445	CCS	1,0–0,1
11280.006	HC_7N	10–9
11561.513	CCCS	2–1
12162.979	OCS	1–0
12178.593	CH_3OH	2(0,2)–3(−1,3) E
12408.003	HC_7N	11–10
12782.769	HC_9N	22–21
12848.48	Unidentified	
12848.731	$HC^{11}N$	38–37
13043.814	SO	1(2)–1(1)
13116.451	Unidentified	
13116.569	Unidentified	
13186.46	Unidentified	
13186.853	$HC^{11}N$	39–38
13186.98	Unidentified	
13313.312	HC_5N	5–4
13363.801	HC_9N	23–22
13434.596	OH	23/2 J = 7/2 F = 3–3
13441.4173	OH	23/2 J = 7/2 F = 4–4
13535.998	HC_7N	12–11
13778.804	$H_2{}^{13}CO$	2(1,1)–2(1,2)
13880.54	Unidentified	
13944.832	HC_9N	24–23
14488.4589	H_2CO	2(1,1)–2(1,2) F = 1–1
14488.4712	H_2CO	2(1,1)–2(1,2) F = 1–2
14488.4801	H_2CO	2(1,1)–2(1,2) F = 3–3
14488.4899	H_2CO	2(1,1)–2(1,2) F = 2–2
14525.862	HC_9N	25–24
14663.993	HC_7N	13–12
14782.212	$^{13}CH_3OH$	2(0,2)–3(−1,3) E
14812.002	c-C_3H	1(1,0)–1(1,1) J = 3/2–1/2 F = 2–1
14877.671	c-C_3H	1(1,0)–1(1,1) J = 3/2–3/2 F = 2–1
14893.050	c-C_3H	1(1,0)–1(1,1) J = 3/2–3/2 F = 2–2
14895.243	c-C_3H	1(1,0)–1(1,1) J = 3/2–3/2 F = 1–1
15106.892	HC_9N	26–25
15248.225	C_6H	23/2 J = 11/2–9/2 F = 6–5 f
15248.359	C_6H	23/2 J = 11/2–9/2 F = 5–4 f
15249.064	C_6H	23/2 J = 11/2–9/2 F = 6–5 e
15249.198	C_6H	23/2 J = 11/2–9/2 F = 5–4 e
15687.921	HC_9N	27–26
15791.986	HC_7N	14–13
15975.966	HC_5N	6–5
16268.950	HC_9N	28–27
16849.979	HC_9N	29–28
16886.312	DCCCN	2–1 F = 2–1
16886.405	DC_3N	2–1 F = 3–2
16919.979	HC_7N	15–14
17091.742	CH_3CCH	1(0)–0(0)
17342.256	CCCS	3–2
17431.006	HC_9N	30–59
17632.685	$H^{13}CCCN$	2–1 F = 2–2
17633.844	$H^{13}CCCN$	2–1 F = 3–2
17647.479	C_4D	5/2–3/2 F = 5/2–3/2
17647.526	C_4D	5/2–3/2 F = 3/2–1/2
17647.716	C_4D	5/2–3/2 F = 7/2–5/2

(*continued on next page*)

Table 1 (*continued*)

17666.995	$HCCC^{15}N$	2–1
17683.961	C_4D	3/2–1/2 $F = 5/2–3/2$
17684.662	C_4D	3/2–1/2 $F = 3/2–1/2$
17736.75	Unidentified	
17788.570	H_2CCCC	2(1,2)–1(1,1)
17863.803	H_2CCCC	2(0,2)–1(0,1)
17937.956	H_2CCCC	2(1,1)–1(1,0)
17945.85	Unidentified	
17951.95	Unidentified	
17965.09	Unidentified	
17974.01	Unidentified	
18012.033	HC_9N	31–30
18012.46	Unidentified	
18017.337	NH_3	7(3)–7(3)
18020.574	C_6H	23/2 $J = 6.5–5.5$ $F = 7–6$ e
18020.644	C_6H	23/2 $J = 6.5–5.5$ $F = 6–5$ e
18021.752	C_6H	23/2 $J = 6.5–5.5$ $F = 7–6$ f
18021.818	C_6H	23/2 $J = 6.5–5.5$ $F = 6–5$ f
18021.86	Unidentified	
18047.969	HC_7N	16–15
18119.029	$HC^{13}CCN$	2–1 $F = 2–1$
18120.773	$HCC^{13}CN$	2–1 $F = 2–1$
18120.865	$HCC^{13}CN$	2–1 $F = 3–2$
18154.884	SiS	1–0
18186.652	C_8H	23/2 15.5–15.5 e
18186.782	C_8H	23/2 15.5–15.5 f
18194.9206	HCCCN	2–1 $F = 2–2$
18195.3176	HCCCN	2–1 $F = 1–0$
18196.2183	HCCCN	2–1 $F = 2–1$
18196.3119	HCCCN	2–1 $F = 3–2$
18197.078	HCCCN	2–1 $F = 1–2$
18198.3756	HCCCN	2–1 $F = 1–1$
18222.65	Unidentified	
18285.434	NH_3	10(7)–10(7)
18294.20	Unidentified	
18299.5	Unidentified	
18306.3	Unidentified	
18320.7	Unidentified	
18343.144	c-C_3H_2	1(1,0)–1(0,1)
18360.50	Unidentified	
18363.045	Unidentified	
18363.142	Unidentified	
18363.306	Unidentified	
18363.406	Unidentified	
18368.0	Unidentified	
18379.6	Unidentified	
18383.3	Unidentified	
18391.562	NH_3	6(1)–6(1)
18396.7252	CH_3CN	1(0)–0(0) $F = 1–1$
18397.9965	CH_3CN	1(0)–0(0) $F = 2–1$
18399.8924	CH_3CN	1(0)–0(0) $F = 0–1$
18413.822	c-$H^{13}CCCH$	1(1,0)–1(0,1)
18422.00	Unidentified	
18485.07	Unidentified	
18494.1	CH_3SH	18(2)–17(3) A+
18499.390	NH_3	9(6)–9(6)
18513.316	CH_2CHCN	2(1,2)–1(1,1) $F = 3–2$
18586.06	Unidentified	
18593.060	HC_9N	32–31
18638.616	HC_5N	7–6
18650.308	HCCCHO	2(0,2)–1(0,1)
18673.312	HNCCC	2–1
18698.16	Unidentified	
18729.12	Unidentified	
18793.92	Unidentified	
18802.235	$H_2CCCCCC$	7(1,7)–6(1,6)
18807.888	NH_2D	3(1,3)–3(0,3)
18808.507	NH_3	8(5)–8(5)
18817.66	Unidentified	
18864.65	Unidentified	
18884.695	NH_3	6(2)–6(2)
18907.54	Unidentified	
18918.50	Unidentified	
18961.79	Unidentified	
18965.588	CH_2CHCN	2(0,2)–1(0,1) $F = 1–0$
18966.535	CH_2CHCN	2(0,2)–1(0,1) $F = 2–1$
18966.616	CH_2CHCN	2(0,2)–1(0,1) $F = 3–2$
18968.48	Unidentified	
18986.20	Unidentified	
19014.7204	C_4H	5/2–3/2 $F = 2–1$
19015.1435	C_4H	5/2–3/2 $F = 3–2$
19025.107	C_4H	5/2–3/2 $F = 2–2$
19039.50	Unidentified	
19043.0	Unidentified	
19044.760	C_4H	3/2–1/2 $F = 1–1$
19054.4762	C_4H	3/2–1/2 $F = 2–1$
19055.9468	C_4H	3/2–1/2 $F = 1–0$
19099.656	C_4H	3/2–3/2 $F = 1–1$
19119.764	C_4H	$J = 3/2–3/2$ $F = 2–2$
19174.086	HC_9N	33–32
19175.958	HC_7N	17–16
19218.465	NH_3	7(4)–7(4)
19243.521	CCCO	2–1
19262.140	CH_3CHO	1(0,1)–0(0,0) E
19265.137	CH_3CHO	1(0,1)–0(0,0) A++
19316.70	Unidentified	
19325.20	Unidentified	
19336.10	Unidentified	
19361.50	Unidentified	
19418.661	c-C_3HD	1(1,0)–1(0,1) $F = 1–1$
19418.686	c-C_3HD	1(1,0)–1(0,1) $F = 2–1$
19418.712	c-C_3HD	1(1,0)–1(0,1) $F = 1–2$
19418.724	c-C_3HD	1(1,0)–1(0,1) $F = 0–1$
19418.740	c-C_3HD	1(1,0)–1(0,1) $F = 2–2$
19418.796	c-C_3HD	1(1,0)–1(0,1) $F = 1–0$
19426.679	CH_2CHCN	2(1,1)–1(1,0) $F = 2–1$
19427.851	CH_2CHCN	2(1,1)–1(1,0) $F = 3–2$
19429.098	CH_2CHCN	2(1,1)–1(1,0) $F = 1–0$
19430.85	Unidentified	
19609.78	Unidentified	
19682.50	Unidentified	

(*continued on next page*)

Table 1 (*continued*)

Frequency (MHz)	Formula	Quantum numbers
19692.50	Unidentified	
19755.111	HC_9N	34–33
19757.538	NH_3	6(3)–6(3)
19771.50	Unidentified	
19780.800	CCCN	2–1 $J = 5/2–3/2$ $F = 5/2–3/2$
19780.826	CCCN	2–1 $J = 5/2–3/2$ $F = 3/2–1/2$
19781.094	CCCN	2–1 $J = 5/2–3/2$ $F = 7/2–5/2$
19799.951	CCCN	2–1 $J = 5/2–3/2$ $F = 3/2–1/2$
19800.121	CCCN	2–1 $J = 5/2–3/2$ $F = 5/2–3/2$
19838.346	NH_3	5(1)–5(1)
19871.344	HCCNC	2–1
19967.396	CH_3OH	2(1,1)–3(0,3) E
19974.50	Unidentified	
20064.21	Unidentified	
20109.547	CH_2CN	1–0 3/2–1/2 5/2–3/2 5/2–5/2
20115.77	CH_2CN	1–0 1/2–1/2 3/2–3/2 5/2–5/2
20117.43	CH_2CN	1–0 3/2–1/2 5/2–3/2 3/2–1/2
20118.014	CH_2CN	1–0 3/2–1/2 5/2–3/2 5/2–3/2
20118.16	CH_2CN	1–0 3/2–1/2 1/2–1/2 3/2–3/2
20119.606	CH_2CN	1–0 3/2–1/2 5/3–3/2 7/2–5/2
20121.61	CH_2CN	1–0 3/2–1/2 3/2–3/2 3/2–3/2
20123.96	CH_2CN	1–0 3/2–1/2 1/2–1/2 3/2–3/2
20124.22	CH_2CN	1–0 1/2–1/2 3/2–1/2 3/2–1/2
20124.22	CH_2CN	1–0 3/2–1/2 3/2–3/2 1/2–1/2
20124.45	CH_2CN	1–0 3/2–1/2 3/2–1/2 3/2–3/2
20124.49	CH_2CN	1–0 1/2–1/2 3/2–3/2 5/2–3/2
20126.031	CH_2CN	1–0 3/2–1/2 3/2–3/2 3/2–1/2
20128.770	CH_2CN	1–0 1/2–1/2 3/2–1/2 3/2–3/2
20139.76	CH_2CN	1–0 1/2–1/2 1/2–3/2 3/2–5/2
20168.48	Unidentified	
20171.089	CH_3OH	11(1,11)–10(2,8) A+
20203.31	Unidentified	
20209.209	CH_2CO	1(0,1)–0(0,0)
20281.00	Unidentified	
20303.946	HC_7N	18–17
20336.135	HC_9N	35–34
20357.226	CH_3C_4H	5(1)–4(1)
20357.423	CH_3C_4H	5(0)–4(0)
20371.45	NH_3	5(2)–5(2)
20460.01	HDO	3(2,1)–4(1,4)
20501.5	Unidentified	
20533.235	Unidentified	
20533.289	C_8H	23/2 17.5–16.5
20723.5	Unidentified	
20728.67	Unidentified	
20735.452	NH_3	9(7)–9(7)
20765.80	Unidentified	
20790.00	Unidentified	
20792.563	H_2CCC	1(0,1)–0(0,0)
20792.872	C_6H	23/2 $J = 15/2–13/2$ $F = 8–7$ e
20792.945	C_6H	23/2 $J = 15/2–13/2$ $F = 7–6$ e
20794.444	C_6H	23/2 $J = 15/2–13/2$ $F = 8–7$ f
20794.512	C_6H	23/2 $J = 15/2–13/2$ $F = 7–6$ f
20804.830	NH_3	7(5)–7(5)
20838.20	Unidentified	
20847.50	Unidentified	
20852.527	NH_3	10(8)–10(8)
20878.00	Unidentified	
20908.848	CH_3OH	16(−4,13)–15(−5,10) E
20917.157	HC_9N	36–35
20970.658	CH_3OH	10(1,10)–11(,9) A+ $t = 1$
20994.617	NH_3	6(4)–6(4)
20999.79	Unidentified	
21070.739	NH_3	11(9)–11(9)
21134.311	NH_3	4(1)–4(1)
21143.18	Unidentified	
21231.00	Unidentified	
21285.275	NH_3	5(3)–5(3)
21301.261	HC_5N	8–7
21322.50	Unidentified	
21431.932	HC_7N	19–18
21447.8	Unidentified	
21453.93	Unidentified	
21470.4	Unidentified	
21480.809	C_5H	21/2 $J = 9/2–7/2$ $F = 5–4$ e
21481.299	C_5H	21/2 $J = 9/2–7/2$ $F = 4–3$ e
21484.695	C_5H	21/2 $J = 9/2–7/2$ $F = 5–4$ f
21485.248	C_5H	21/2 $J = 9/2–7/2$ $F = 4–3$ f
21488.255	$H_2CCCCCC$	8(1,8)–7(1,7)
21498.182	HC_9N	37–36
21546.94	Unidentified	
21550.342	CH_3OH	12(2,11)–11(1,11) A+ $t = 1$
21569.5	Unidentified	
21576.5	Unidentified	
21582.6	Unidentified	
21587.400	c-C_3H_2	2(2,0)–2(1,1)
21592.1	Unidentified	
21595.8	Unidentified	
21598.4	Unidentified	
21606.30	Unidentified	
21615.5	Unidentified	
21703.3580	NH_3	4(2)–4(2)
21715.8	Unidentified	
21930.476	$CC^{34}S$	2,1–1,0
21980.5453	HNCO	1(0,1)–0(0,0) $F = 0–1$
21981.4706	HNCO	1(0,1)–0(0,0) $F = 2–1$
21982.0854	HNCO	1(0,1)–0(0,0) $F = 1–1$
22079.204	HC_9N	38–37
22235.044	H_2O	6(1,6)–5(2,3) $F = 7–6$
22235.077	H_2O	6(1,6)–5(2,3) $F = 6–5$
22235.120	H_2O	6(1,6)–5(2,3) $F = 5–4$
22235.253	H_2O	6(1,6)–5(2,3) $F = 6–6$
22235.298	H_2O	6(1,6)–5(2,3) $F = 5–5$
22258.173	CCO	2,1–1,0
22307.670	HDO	5(3,2)–5(3,3)
22344.030	CCS	2,1–1,0
22471.180	HCOOH	1(0,1)–0(0,0)
22559.915	HC_7N	20–19

(*continued on next page*)

Table 1 (*continued*)

22624.8892	$^{15}NH_3$	1(1)–1(1) *F*,*F*1=1.5,1–1.3,1
22624.9331	$^{15}NH_3$	1(1)–1(1) *F*,*F*1=1.5,1–0.8,1
22624.9410	$^{15}NH_3$	1(1)–1(1) *F*,*F*1=0.5,1–0.8,1
22624.9469	$^{15}NH_3$	1(1)–1(1) *F*,*F*1=1.5,2–1.5,2
22639.3	Unidentified	
22644.3	Unidentified	
22649.843	$^{15}NH_3$	2(2)–2(2)
22653.022	NH_3	5(4)–5(4)
22660.225	HC_9N	39–38
22678.6	Unidentified	
22688.312	NH_3	4(3)–4(3)
22732.429	NH_3	6(5)–6(5)
22789.421	$^{15}NH_3$	3(3)–3(3)
22827.741	CH_3OCHO	2(1,2)–1(1,1) E
22828.134	CH_3OCHO	2(1,2)–1(1,1) A
22834.1851	NH_3	3(2)–3(2)
22878.949	DC5N	9–8
22924.940	NH_3	7(6)–7(6)
23046.0158	$^{15}NH_3$	4(4)–4(4)
23098.8190	NH_3	2(1)–2(1)
23121.024	CH_3OH	9(2,7)–10(1,10) A+
23122.983	CCCS	4–3
23142.2	Unidentified	
23228.0	Unidentified	
23232.238	NH_3	8(7)–8(7)
23241.246	HC_9N	40–39
23421.9823	$^{15}NH_3$	5(5)–5(5)
23444.778	CH_3OH	10(1,9)–9(2,8) A–
23565.160	C_6H	23/2 *J* = 17/2–15/2 *F* = 9–8 e
23565.226	C_6H	23/2 *J* = 17/2–15/2 *F* = 8–7 e
23567.169	C_6H	23/2 *J* = 17/2–15/2 *F* = 9–8 f
23567.238	C_6H	23/2 *J* = 17/2–15/2 *F* = 8–7 f
23600.242	SiC_2	1(0,1)–0(0,0)
23657.471	NH_3	9(8)–9(8)
23687.898	HC_7N	21–20
23692.9265	NH_3	1(1)–1(1) *F*,*F*1=1/2,1–1/2,0
23692.9688	NH_3	1(1)–1(1) *F*,*F*1=3/2,1–1/2,0
23693.8722	NH_3	1(1)–1(1) *F*,*F*1=1/2,1–3/2,2
23693.9051	NH_3	1(1)–1(1) *F*,*F*1=3/2,1–5/2,2
23693.9145	NH_3	1(1)–1(1) *F*,*F*1=3/2,1–3/2,2
23694.4591	NH_3	1(1)–1(1) *F*,*F*1=1/2,1–1/2,1
23694.4700	NH_3	1(1)–1(1) *F*,*F*1=1/2,1–3/2,1
23694.4709	NH_3	1(1)–1(1) *F*,*F*1=3/2,2–5/2,2
23694.4803	NH_3	1(1)–1(1) *F*,*F*1=3/2,2–3/2,2
23694.5014	NH_3	1(1)–1(1) *F*,*F*1=3/2,1–1/2,1
23694.5060	NH_3	1(1)–1(1) *F*,*F*1=5/2,2–5/2,2
23694.5123	NH_3	1(1)–1(1) *F*,*F*1=3/2,1–3/2,1
23694.5153	NH_3	1(1)–1(1) *F*,*F*1=5/2,2–3/2,2
23695.0672	NH_3	1(1)–1(1) *F*,*F*1=3/2,2–3/2,1
23695.0782	NH_3	1(1)–1(1) *F*,*F*1=3/2,2–3/2,1
23695.1132	NH_3	1(1)–1(1) *F*,*F*1=5/2,2–3/2,1
23696.0297	NH_3	1(1)–1(1) *F*,*F*1=1/2,0–1/2,1
23696.0406	NH_3	1(1)–1(1) *F*,*F*1=1/2,0–3/2,1
23697.9	Unidentified	
23718.325	$HC^{13}CCCCN$	9–8

Table 1 (*continued*)

23720.575	NH_3	2(2)–2(2) *F*1 = 1–2
23721.336	NH_3	2(2)–2(2) *F*1 = 3–2
23722.6323	NH_3	2(2)–2(2) *F*1 = 2–2
23722.6336	NH_3	2(2)–2(2) *F*1 = 3–3
23722.6344	NH_3	2(2)–2(2) *F*1 = 1–1
23723.929	NH_3	2(2)–2(2) *F*1 = 2–3
23724.691	NH_3	2(2)–2(2) *F*1 = 2–1
23727.162	$HCCCC^{13}CN$	9–8
23804.5	Unidentified	
23811.0	Unidentified	
23817.6153	OH	23/2 *J* = 9/2 *F* = 4–4
23822.265	HC_9N	41–40
23826.6211	OH	23/2 *J* = 9/2 *F* = 5–5
23867.805	NH_3	3(3)–3(3) *F*1 = 2–3
23868.450	NH_3	3(3)–3(3) *F*1 = 4–3
23870.1279	NH_3	3(3)–3(3) *F*1 = 3–3
23870.1296	NH_3	3(3)–3(3) *F*1 = 4–4
23870.1302	NH_3	3(3)–3(3) *F*1 = 2–2
23871.807	NH_3	3(3)–3(3) *F*1 = 3–4
23872.453	NH_3	3(3)–3(3) *F*1 = 3–2
23922.3132	$^{15}NH_3$	6(6)–6(6)
23939.089	$HCC^{13}CCCN$	9–8
23941.99	$HCCC^{13}CCN$	9–8
23959.5	Unidentified	
23963.901	HC_5N	9–8
23987.5	Unidentified	
23990.2	Unidentified	
23996.7	Unidentified	
24004.5	Unidentified	
24023.2	Unidentified	
24037.1	Unidentified	
24048.5	Unidentified	
24139.4169	NH_3	4(4)–4(4)
24205.287	NH_3	10(9)–10(9)
24296.491	CH_3OCHO	2(0,2)–1(0,1) E
24298.481	CH_3OCHO	2(0,2)–1(0,1) A
24325.927	OCS	2–1
24375.2	Unidentified	
24428.652	CH_3C_4H	6(1)–5(1)
24428.886	CH_3C_4H	6(0)–5(0)
24532.9887	NH_3	5(5)–5(5)
24788.541	CH_3CCCN	6(1)–5(1)
24788.780	CH_3CCCN	6(0)–5(0)
24815.878	HC_7N	22–21
24928.715	CH_3OH	3(2,1)–3(1,2) E
24933.468	CH_3OH	4(2,2)–4(1,3) E
24934.382	CH_3OH	2(2,0)–2(1,1) E
24959.079	CH_3OH	5(2,3)–5(1,4) E
24984.302	HC_9N	43–42
24991.19	SiC2	8(2,6)–8(2,7)
25018.123	CH_3OH	6(2,4)–6(1,5) E
25023.792	NH_2D	4(1,4)–4(0,4)
25056.025	NH_3	6(6)–6(6)
25124.872	CH_3OH	7(2,5)–7(1,6) E
25249.938	C5N	21/2 *N* = 9–8 *J* = 9.5–8.5

(*continued on next page*)

Table 1 (*continued*)

Frequency (MHz)	Formula	Quantum numbers
25260.649	C5N	21/2 N = 9–8 J = 8.5–7.5
25294.417	CH_3OH	8(2,6)–8(1,7) E
25329.441	DC_3N	3–2
25421.036	DC5N	10–9
25541.398	CH_3OH	9(2,7)–9(1,8) E
25715.182	NH_3	7(7)–7(7)
25878.266	CH_3OH	10(2,8)–10(1,9) E
25911.017	CCS	2,2–1,1
25943.855	HC_7N	23–22
26337.414	C_6H	23/2 J = 19/2–17/2 F = 10–9 f
26337.463	C_6H	23/2 J = 19/2–17/2 F = 9–8 f
26339.924	C_6H	23/2 J = 19/2–17/2 F = 10–9 e
26339.973	C_6H	23/2 J = 19/2–17/2 F = 9–8 e
26363.491	$HCCCC^{13}CN$	10–9
26450.598	$H^{13}CCCN$	3–2
26500.462	$HCCC^{15}N$	3–2
26518.981	NH_3	8(8)–8(8)
26602.181	$HCCC^{13}CCN$	10–9
26626.533	HC_5N	10–9
26682.814	H_2CCCC	3(1,3)–2(1,2)
26795.635	H_2CCCC	3(0,3)–2(0,2)
26847.205	CH_3OH	12(2,10)–12(1,11) E
26906.891	H_2CCCC	3(1,2)–2(1,1)
27071.824	HC_7N	24–23
27084.348	c-C_3H_2	3(3,0)–3(2,1)
27178.511	$HC^{13}CCN$	3–2
27181.127	$HCC^{13}CN$	3–2
27292.903	HCCCN	3–2 F = 3–3
27294.078	HCCCN	3–2 F = 2–1
27294.295	HCCCN	3–2 F = 3–2
27294.347	HCCCN	3–2 F = 4–3
27296.235	HCCCN	3–2 F = 2–2
27472.501	CH_3OH	13(2,11)–13(1,12) E
27477.943	NH_3	9(9)–9(9)
28009.975	HNCCC	3–2
28169.437	CH_3OH	14(2,12)–14(1,13) E
28199.804	HC_7N	25–24
28199.805	HC_7N	25–24
28316.031	CH_3OH	4(0,4)–3(1,2) E
28440.980	CH_2CHCN	3(0,3)–2(0,2)
28470.391	HC_9N	49–48
28532.31	C_4H	7/2–5/2 F = 3–2
28532.46	C_4H	7/2–5/2 F = 4–3
28542.284	C_4H	J = 5/2–5/2 F = 3–3
28571.37	C_4H	5/2–3/2 F = 3–2
28571.53	C_4H	5/2–3/2 F = 2–1
28604.737	NH_3	10(10)–10(10)
28903.688	CCCS	5–4
28905.787	CH_3OH	15(2,13)–12(1,14) E
28919.931	CH_3CCCN	7(1)–6(1)
28920.209	CH_3CCCN	7(0)–6(0)
28969.954	CH_3OH	8(2,7)–9(1,8) A–
28974.781	H_2CO	3(1,2)–3(1,3) F = 2–2
28974.804	H_2CO	3(1,2)–3(1,3) F = 4–4
28974.814	H_2CO	3(1,2)–3(1,3) F = 3–3
28999.814	$HCCCC^{13}CN$	11–10
29051.403	HC_9N	50–49
29109.644	C_6H	23/2 J = 21/2–19/2 F = 11–10 f
29109.66	C_6H	23/2 J = 21/2–19/2 f
29109.686	C_6H	23/2 J = 21/2–19/2 F = 10–9 f
29112.709	C_6H	23/2 J = 21/2–19/2 F = 11–10 f
29112.73	C_6H	23/2 J = 21/2–19/2 e
29112.750	C_6H	23/2 J = 21/2–19/2 F = 10–9 f
29138.877	CH_2CHCN	3(1,2)–2(1,1) F = 3–2
29139.215	CH_2CHCN	3(1,2)–2(1,1) F = 4–3, 2–1
29258.834	$HCC^{13}CCCN$	11–10
29289.159	HC_5N	11–10
29304.09	C_6H	21/2 J = 21/2–19/2 e
29310.5	Unidentified	
29327.776	HC_7N	26–25
29332.45	C_6H	21/2 J = 21/2–19/2 f
29333.3	Unidentified	
29337.57	HC_5N	11–10 $v11$ = 1 = 1c
29342.0	Unidentified	
29353.8	Unidentified	
29363.15	HC_5N	11–10 $v11$ = 1 = 1d
29365.0	Unidentified	
29477.704	CCS	2,3–1,2
29632.406	HC_9N	51–50
29632.413	HC_9N	51–50
29636.920	CH_3OH	16(2,14)–12(1,15) E
29676.14	CCCN	3–2 J = 7/2–5/2 F = 7/2–5/2
29676.28	CCCN	3–2 J = 7/2–5/2 F = 9/2–7/2
29678.882	^{34}SO	1(0)–0(1)
29694.99	CCCN	3–2 J = 5/2–3/2 F = 3/2–1/2
29695.14	CCCN	3–2 J = 5/2–3/2 F = 7/2–5/2
29806.963	HCCNC	3–2
29914.486	NH_3	11(11)–11(11)

within an envelope of an AGB star and survived ejection into interstellar space or if they were incorporated onto dust grains and later evaporated from their surfaces upon exposure to interstellar UV radiation. It is likely that the true situation will be a mixture of both of these cases.

A number of molecules with transitions in the frequency range of the SKA are of particular interest for astrobiology. These include the building block molecule for simple sugars such as ribose and deoxyribose, Furan (C_4H_4O; e.g. with a transition at 10.6 GHz) (Dickens et al., 2001). The same authors detected c-C_2H_4O, one of the few cyclic molecules in space. They note that the presence of these molecular species in cold dark clouds suggests that rather complex organic molecules may have been present in the solar system before the planets formed, a first step toward explaining the origin of life on the early Earth.

5. Magnetic fields

Magnetic fields of AGB stars are now thought to be fairly strong from observations of SiO masers (Kemball and Diamond, 1997). Depending on the exact models used, the field strengths seem to be between 5 and 10 G at radii of 3 AU or so. Such strong magnetic fields will have obvious impacts on both the molecular gas (Zeeman splitting for a number of species such as CCS and SO) and possibly produce circularly polarized radio emission from the star itself (analogous to the emission observed from the Sun). Although requiring careful instrumental polarization characterization, observations of these effects will provide confirmation of the magnetic field strength implied by the SiO maser polarization observations and further constraints on AGB stars themselves. Potential movies of regions of magnetic field enhancements on the surfaces of nearby AGB stars could be tracked with time, testing maser observations of rotation.

6. Molecular line transitions available to the SKA

See Table 1.

Uncited reference

Reid and Menten (1997).

References

Bieging, J.H., Rieu, N.Q., 1996. AJ 112, 706.
Boboltz, D.A., Marvel, K.B., 2000. AJ 545, 149.
Dickens, J.E., Irvine, W.M., Nummelin, A., Mollendal, H., Saito, S., Thorwith, S., Hjalmarsoni, A., Ohishi, M., 2001. Spectrochim. Acta Part A 57, 643.
Kemball, A.J., Diamond, P.J., 1997. AJ 481L, 111.
F.J. Lovas, NIST Recommended Rest Frequencies for Observed Interstellar Molecular Microwave Transitions: 2002 Revision, (2002).
Messenger, S., Keller, L.P., Stadermann, F.J., Walker, R.M., Zinner, E., 2003. Science 300, 105.
Monnier, J.D., Millan-Gabet, R., Tuthill, P.G., Traub, W.A., Carleton, N.P., Coudé du Foresto, V., Danchi, W.C., Lacasse, M.G., Morel, S., Perrin, G., Porro, I.L., Schloerb, C.H., Townes, C.H., 2004. AJ 605, 436.
Monnier, J.D., Tuthill, P.G., Lopez, B., Cruzalebes, P., Danchi, C.A., Haniff, C.A., 1999. AJ 512, 351.
Murakawa, K., Yates, J.A., Richards, A.M.S., Cohen, R.J., . Mon. Not. R. Astron. Soc. 344, 1.
Olofsson, H., Bergman, P., Lucas, R., Eriksson, K., Gustafsson, B., Bieging, J.H., 1998. AstAp 330, L1.
Petit, E., Nicholson, S.B., 1933. AJ 78, 320.
Reid, M.J., Menten, K.M., 1997. AJ 456, 327.
Reid, M.J., Goldston, J.E., 2002. AJ 568, 931.
Reid, M.J., 2002. Cosmic Masers: From Protostars to Blackholes. Astronomical Society of the Pacific.
Richards, A.M.S., Yates, J.A., Cohen, R.J., 1999. Mon. Not. R. Astron. Soc. 306, 954.
Richards, A.M.S., Yates, J.A., Cohen, R.J., 1998. Mon. Not. R. Astron. Soc. 299, 319.
Rieu, N.Q., Bieging, J.H., 1990. AJ 359, 131.
Taylor, A.R., Braun, R., 1999. Science with the Square Kilometer Array.
Zijlstra A.A., 2003. In: Kramer, Rawlings (Eds.). The Scientific Promise of the SKA: SKA Workshop Oxford. Available from: http://www.skatelescope.org/documents/Workshop_Oxford2002.pdf.